J Biomol NMR (2011) 51:497–504
DOI 10.1007/s10858-011-9580-7

ARTICLE

Speeding up direct ^{15}N detection: hCaN 2D NMR experiment

Maayan Gal · Katherine A. Edmonds · Alexander G. Milbradt · Koh Takeuchi · Gerhard Wagner

Received: 9 August 2011 / Accepted: 11 October 2011 / Published online: 30 October 2011

Abstract Experiments detecting low gyromagnetic nuclei have recently been proposed to utilize the relatively slow relaxation properties of these nuclei in comparison to ^{1}H. Here we present a new type of ^{15}N direct-detection experiment. Like the previously proposed CaN experiment (Takeuchi et al. in J Biomol NMR 47:271–282, 2010), the hCaN experiment described here sequentially connects amide ^{15}N resonances, but utilizes the initial high polarization and the faster recovery of the ^{1}H nucleus to shorten the recycling delay. This allows recording 2D ^{15}N-detected NMR experiments on proteins within a few hours, while still obtaining superior resolution for ^{13}C and ^{15}N, establishing sequential assignments through prolines, and at conditions where amide protons exchange rapidly. The experiments are demonstrated on various biomolecules, including the small globular protein GB1, the 22 kDa HEAT2 domain of eIF4G, and an unstructured polypeptide fragment of NFAT1, which contains many SerPro sequence repeats.

Katherine A. Edmonds and Alexander G. Milbradt have contributed equally.

Electronic supplementary material The online version of this article (doi:10.1007/s10858-011-9580-7) contains supplementary material, which is available to authorized users.

M. Gal · K. A. Edmonds · A. G. Milbradt · G. Wagner (✉)
Department of Biochemistry and Molecular Pharmacology, Harvard Medical School, 240 Longwood Avenue, Boston, MA 02115, USA
e-mail: gerhard_wagner@hms.harvard.edu

K. Takeuchi
Biomedicinal Information Research Center, National Institute of Advanced Industrial Science and Technology, Tokyo 135-0064, Japan

Keywords ^{15}N direct detection · CaN · hCaN · Nuclear magnetic resonance (NMR)

Introduction

One of the current challenges in biomolecular NMR spectroscopy is improving sensitivity and resolution in cases where severe line broadening hinders NMR spectra acquisition due to fast transverse relaxation of the spins of interest. This occurs in high molecular-weight systems where the slow tumbling of the biomolecule results in a fast decay of coherences. Fast transverse relaxation is also observed in chemical exchange of two or more states, where the swapping of different frequencies or coupling constants during chemical shift encoding leads to line broadening (Cavanagh et al. 1996; Levitt 2001). An additional problem arises for experiments that rely on amide-proton detection at high pH, and for solvent-exposed groups, in particular for unstructured proteins or protein segments. As NH exchange is base-catalyzed above pH 4 (Wuthrich and Wagner 1979), exposed peptide protons are typically not observable above pH 8. Similarly, paramagnetic systems exhibit very fast relaxation of the spins near the paramagnetic center, such that ^{1}H detection is often not possible (Bertini et al. 2008).

Several NMR experimental schemes have been proposed to overcome these issues of line-broadening, enabling the acquisition of NMR data for the systems described above. Signal losses in high molecular weight proteins result mainly from intensive ^{1}H–^{1}H dipolar interactions during slow tumbling. This can be diminished by expressing proteins in deuterated media to exchange all the ^{1}H in the protein with ^{2}H (Venters et al. 1995). In addition, TROSY NMR spectroscopy enables detection of

long-lived coherences even in very high molecular weight systems (Pervushin et al. 1997; Pervushin 2000; Tugarinov et al. 2003).

A different approach to deal with line broadening in NMR is the detection of low-γ nuclei, which has been extensively developed in recent years mainly in the context of direct ^{13}C detection (Lee et al. 2005; Bermel et al. 2006a, c; Takeuchi et al. 2008; Felli and Brutscher 2009). Low-γ nuclei detection can facilitate NMR data acquisition of complex systems by observing the naturally longer-lived coherences of such nuclei. Although ^{13}C detection methods have become the primary alternative detection to ^{1}H in biomolecular NMR for assignment and structure calculations, ^{15}N detection experiments have been proposed as well for this purpose (Takeuchi et al. 2010). It was recently shown that ^{15}N direct detection can also provide valuable information on protein backbone dynamics. Dissolving the protein in D_2O-based buffer permits accurate CSA values to be determined directly on ^{15}N without being masked by the extensive ^{1}H dipolar interaction of the directly attached proton (Xu et al. 2005; Vasos et al. 2006). Moreover, although outside the scope of current biomolecular NMR applications, ^{15}N detection experiments were used quite some time ago (Levy and Lichter 1979).

Another advantage associated with direct ^{13}C and ^{15}N detection is the ability to assign and obtain spectral information on proline residues, which are otherwise difficult to detect in conventional HN-based NMR methods. This is important for studying unstructured proteins or protein segments, which often have proline-rich regions in their primary structure (Tompa 2003; Bermel et al. 2006b). To target unstructured proteins with NMR, new proton-detected methods have recently been proposed (Mantylahti et al. 2010) and can assist in backbone assignments (Tamiola and Mulder 2011). Combining these methods with low-γ nuclei detection will facilitate investigation of such systems under a broader range of conditions. In particular, ^{15}N detection offers higher resolution because of the wider ^{15}N frequency dispersion. Another advantage of low γ detection is that there is no need for water suppression, which is an everlasting problem in ^{1}H detected experiments.

Naturally, the main problem of direct ^{13}C and ^{15}N detection is the lower inherent sensitivity due to the lower gyromagnetic ratio (γ) of the acquired spin. A loss factor of $(\gamma_H/\gamma_I)^2$ originates from the smaller magnetic moment and lower precession frequency of nucleus I (^{13}C or ^{15}N) relative to ^{1}H. In addition, another loss of (γ_H/γ_I) occurs if the experimental design starts from a low-γ nucleus, due to the smaller thermal equilibrium polarization (Hoult 1978; Howarth and Lilley 1978). One of the most common experimental schemes to enhance low γ detection is J-coupling-mediated transfer of proton nuclear polarization by INEPT (Morris and Freeman 1979). Proposals have been made to extend this enhancement and use proton polarization also during acquisition while actually detecting ^{15}N chemical shifts, which would further narrow the sensitivity difference (Mishkovsky and Frydman 2004). Although these methods are not comparable in signal intensity to proton detection, the narrower line width resulting from slower decay of ^{15}N and ^{13}C signals may in special cases compensate for such losses (Howarth and Lilley 1978). Indeed, an example of such compensation is the success of collecting spectral information by one-dimensional ^{15}N-direct detection experiments on paramagnetic proteins near their active sites which would otherwise be invisible by ^{1}H detection (Vance et al. 1997; John et al. 2007; Lin et al. 2009).

All of these arguments have recently brought Takeuchi et al. (2010) to design the CaN 2D NMR experiment. This experiment can be used to record 2D ^{13}C–^{15}N spectra with direct nitrogen detection, providing superior line widths in both dimensions. The main disadvantage for this kind of experiment is the relatively long time required to sample the NMR spectral grid with a sufficient signal-to-noise ratio (SNR) due to the low ^{15}N γ.

One method for mitigating this effect is to use an experimental scheme that permits a shorter recycle delay in order to increase the number of scans per unit time. For example, relaxation agents such as Gd (DTPA-BMA) or DO2A have been used (Takeuchi et al. 2010) to reduce the effective T_1 relaxation rates without significantly impacting T_2 (Cai et al. 2006).

We describe here a modified version of the original CaN experiment to record a 2D ^{13}C–^{15}N plane. The new hCaN experiment utilizes the high initial proton polarization to achieve better sensitivity by starting the NMR pulse sequence from the Ha nucleus. This enables collecting 2D CaN spectral information with direct detection of ^{15}N nuclei within the span of only a few hours. We have tested the pulse scheme on several proteins of various sizes, and have compared the results with those of the previous CaN experiment.

Materials and methods

All chemicals were purchased from Sigma (St. Louis, MO) unless otherwise noted. All stable-isotope-labeled materials were acquired from Cambridge Isotope laboratories (Cambridge, MA).

Expression and purification of the B1 domain of protein G (GB1)

The gene for the His6-tagged GB1 domain was cloned into the pET9d vector (Novagen, San Diego, CA) as previously described (Zhou et al. 2001). GB1 was expressed in

commercially available BL21 (DE3) *E. coli* cells (Novagen) at 37°C, and protein expression was induced for 6 h at the same temperature. For uniformly $^{15}N^{13}C$-labeled samples, the cells were cultured in $^{15}N^{13}C$ M9 media containing 8.5 g/l Na_2HPO4, 3 g/l KH_2PO_4, 0.5 g/l NaCl, 2 mM $MgCl_2$, 0.1 mM CaCl2 in H_2O supplemented with 2 g/l ^{13}C glucose and 1 g/l of $^{15}NH_4Cl$. The protein was purified by Ni–NTA affinity and size exclusion chromatography as previously described (Frueh et al. 2005).

Expression and purification of the HEAT2 domain

The gene for the HEAT2 domain of human eIF4G (residues 1236-1427) was cloned into a pET21a vector (Novagen, San Diego, CA) with N-terminal GB1 and His8-tags and a TEV protease cleavage site inserted as described elsewhere (Marintchev et al. 2009). HEAT2 was expressed in commercially available BL21 (DE3) *E. coli* cells (Novagen) grown at 37°C in $^{15}N^{13}C$ M9 media, and protein expression was induced overnight at 20°C. The protein was purified by Ni–NTA affinity chromatography, followed by overnight TEV cleavage and size exclusion chromatography, as previously described (Marintchev et al. 2009).

NMR experiments

All ^{15}N detection NMR spectra were recorded on a Bruker (Billerica, MA) Avance spectrometer operating at 500 MHz proton frequency, equipped with a triple-resonance cryogenic probe (TXO) in which the carbon and nitrogen are both on the inner coil and are detected with cryogenic preamplifiers. This design is intended for low-γ nuclei detection experiments. The ^{1}H-detected experiments were recorded on a Varian INOVA 500 MHz spectrometer. All spectra of the uniformly $^{15}N^{13}C$-labeled GB1 sample (2.5 mM) were recorded at 25°C in buffer containing 30 mM sodium phosphate (pH 6.8) with 30 mM NaCl in D_2O. The HEAT2 domain was dissolved in H_2O-based buffer containing 20 mM Tris at pH 7.0, 150 mM NaCl, 1 mM DTT, 0.5 mM EDTA, at a concentration of 1 mM. Unless otherwise noted, all offsets during the following pulse sequence execution were centered at frequencies of 55, 122 and 5 ppm for ^{13}C, ^{15}N and ^{1}H, respectively.

Results

We present here an experimental scheme that enables recording ^{13}Ca–^{15}N 2D NMR spectra of proteins within a few hours while using direct ^{15}N detection. Figure 1a shows a schematic representation of the nuclei participating in the coherence pathways in a pair of neighboring amino acids. Starting from H^i_a, magnetization is transferred to the adjacent alpha carbon, C^i_a, for ω_1 encoding. From C^i_a, coherence is then transferred to N^i and N^{i+1} for direct ^{15}N detection. This last transfer step depends on the transfer duration, as was previously described by Takeuchi et al. (2010). A delay of 22 ms is optimal for simultaneous intra- and inter-residue coherence transfer to N^i and N^{i+1}, respectively. On the other hand, 70 ms is an optimal delay for selecting magnetization transfer to the N^{i+1} while suppressing intra-residue transfer. These options enable acquisition of 2D spectral information

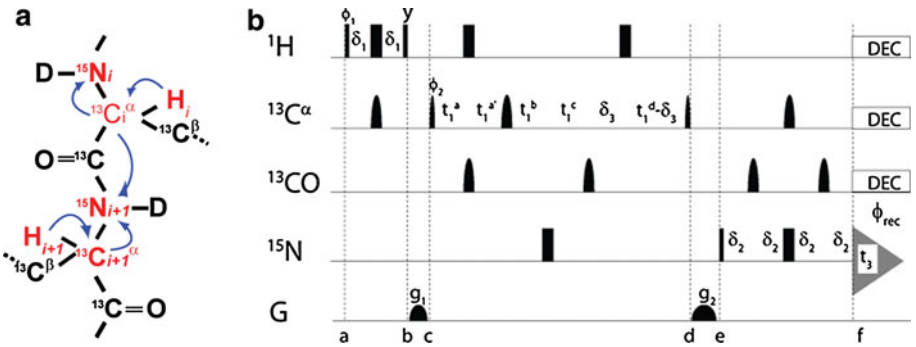

Fig. 1 Coherence pathway and pulse sequence of the 2D hCaN experiment. **a** Illustration of the amino acids that are correlated by the coherence pathways in the hCaN experiment. The nuclei involved in this experiment are colored in *red*. *Arrows* indicate the coherence transfer steps during the hCaN experiment. **b** Pulse program of the nitrogen-detected 2D hCaN NMR experiment. *Narrow* and *wide bars* indicate $\pi/2$ and π pulses, respectively. *Narrow* and *wide semi-elliptical* shapes on the carbon channel represent $\pi/2$ and π Gaussian cascade pulses selective for the frequencies of aliphatic carbon nuclei (Q5/256 and Q3/205 µs, respectively) (Emsley and Bodenhausen 1992). Carbon decoupling during the acquisition period was achieved by using WURST broadband adiabatic inversion with duration and bandwidth of 5 ms and 200 ppm, respectively (Kupce and Freeman 1995). ^{1}H decoupling was executed by applying WALTZ16 modulation (Shaka and Keeler 1987). All pulses are along the *x*-axis unless otherwise indicated. Phase cycling was $\phi_1 = (x, -x)$, $\phi_{rec} = (x, -x)$. Phase sensitive spectra in the indirect dimension were obtained by incrementing ϕ_2 in a States-TPPI manner (Marion et al. 1989). The time delays as applied were $\delta_1 = 1.7$ ms, $\delta_2 = 5.5$ ms, $\delta_3 = 1.6$ ms. Initially, $t_1^a = t_1^{a'} = 7$ ms, $t_1^b = 2.9$ ms, $t_1^c = 3.9$ ms and $t_1^d = 5.4$ ms, unless otherwise noted. ^{13}C chemical shift encoding was achieved in a constant time manner by incrementing delays t_1^c, t_1^d and decrementing t_1^a, simultaneously. Pulsed field gradients were applied along the *z*-axis for 1.0 ms with an intensity of G = 10 G/cm

that can be used for the assignment of ^{15}N and ^{13}Ca resonances along the protein backbone.

Figure 1b shows the pulse sequence that was executed to record the 2D hCaN spectra. It starts with an INEPT polarization transfer (Morris and Freeman 1979) from Ha to Ca, creating a proton-carbon longitudinal two spin order, H_zC_z (a–b). Subsequently, the chemical shift of the carbon is encoded in a constant time manner and an anti-phase ^{13}C scalar-coupled term is created with respect to ^{15}N. The last INEPT block refocuses the ^{15}N anti-phase magnetization with respect to carbon into ^{15}N single quantum coherence before direct nitrogen detection takes place.

Refocusing of Glycine carbon-proton antiphase terms

As was previously mentioned, carbon antiphase magnetization with respect to protons is refocused during points c–d, as is illustrated in Fig. 1b. This affects glycines differently from all other amino acids, since the alpha carbon of glycine is coupled to two protons (IS_2 system), whereas the rest of the amino acids have only a single proton bound to the alpha carbon (IS system). Figure 2a illustrates the single quantum (SQ) coherence amplitude as a function of evolution time under a scalar J coupling interaction Hamiltonian for IS_2 (dashed) and IS (solid) spin system types, corresponding to glycine residues and all other amino acids, respectively. For both spin types the initial coherence in Fig. 2a at time $\delta 3 = 0$ represents the antiphase term of scalar coupled I (^{13}C) to S (^{1}H). The curve was plotted for a scalar coupling of 145 Hz. It can be seen that when the refocusing period $2\delta 3$ is set to a duration of $1/2J_{CH} = 3.4$ ms, the SQ amplitude of the CH groups is maximized. This is the case at the end of the INEPT block after time point d, when $2\delta_3 = 3.4$ ms. However, at the same time the carbon single quantum coherence corresponding to the glycine residues is at a null. Figure 2b, c illustrate this effect by showing a pair of 2D hCaN NMR spectra with different carbon antiphase refocusing times $2\delta 3$ between points c and d. The spectrum in panel c was recorded with a refocusing time equal to $1/2J_{CH}$ (represented by a vertical line marked c in panel 2a). At this time point, no glycine signals are observable (the dashed square in each panel indicates the glycines' unique chemical shift in the 2D CaN spectra). In contrast, the spectrum in panel b was acquired with a shorter refocusing time of $2\delta_3 = 2.8$ ms (represented by a vertical line marked b in panel 2a), so that both types of spin systems are detected. This kind of fine adjustment allows simultaneous observation of glycines and all other amino acids. Another difference between glycines and the other amino acids is the lack of Ca–Cb coupling evolution during time points c–d. This causes signal sign inversion as represented by the different peak colors and is explained elsewhere (Takeuchi et al. 2010).

Acquisition of hCaN spectra

With these factors in mind, we have tested the hCaN pulse sequence on various biomolecules. First, we sought to compare the 2D hCaN against the conventional proton-detected 3D HCaN experiment on a standard sample of 2.5 mM ^{15}N^{13}C-labeled GB1 domain. Figure 3a shows 2D hCaN ^{15}N detected spectrum (left). At this relatively high protein concentration we can record the 2D ^{13}C–^{15}N correlation spectrum within a short time of 2 h 15 min. The ability to achieve all sequential connectivity information in a 2D sampling grid is unique to low-gamma detection. The equivalent experiment using conventional proton detection has the advantages of providing Ha shifts and additionally dispersing the signals along the third dimension. However, these benefits come at a significant cost of measurement time and resolution in both the ^{15}N and ^{13}C dimensions.

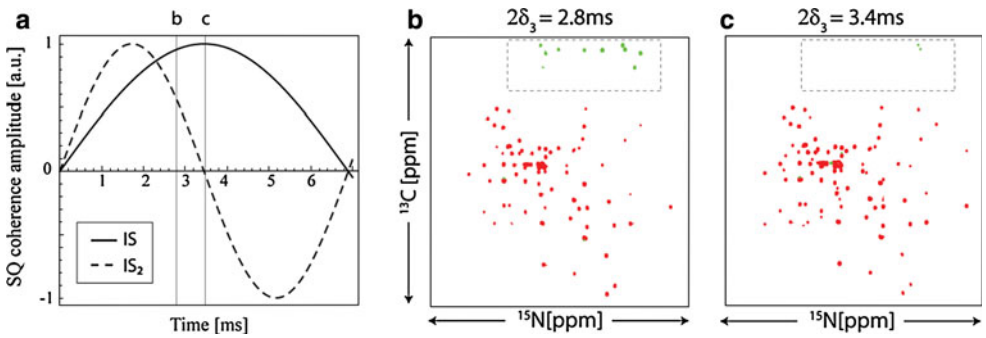

Fig. 2 Glycine ^{1}H–^{13}C anti-phase coherence refocusing. **a** Single quantum coherence amplitude as a function of refocusing time when starting from an antiphase coherence for IS (*solid*) and IS_2 (*dashed*) types of spin systems. The *curves* correspond to a scalar coupling of 145 Hz between nuclei I and S. The *vertical line* at 3.4 ms (marked **c**) indicates a complete refocusing for the IS system and a null for IS_2 system. **b** 2D hCaN spectrum with a short refocusing time of 2.8 ms, resulting in the appearance of glycine signals outlined by the *dashed rectangle*. These peaks are shown in *green* because they have opposite sign due to the lack of Ca–Cb coupling. **c** 2D hCaN spectrum with a 3.4 ms refocusing time $2\delta_3$ optimized for greatest signal intensity of non-glycine residues, and absent glycine signals

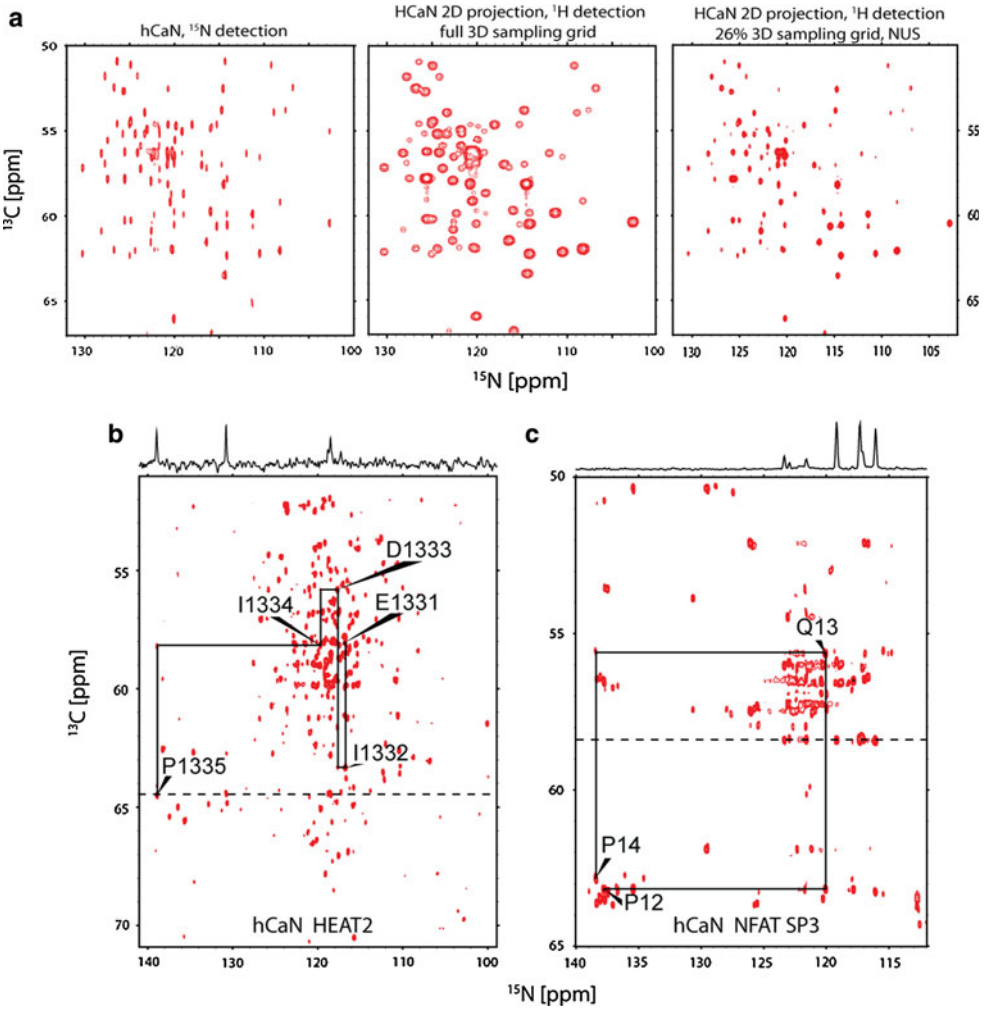

Fig. 3 **a** Comparison of 2D hCaN ^{15}N-detected experiment (*left*) versus 2D projection of 3D HCaN ^{1}H detected experiments acquired using traditional linear sampling (*middle*) and non-uniform sampling (*right*) on uniformly ^{15}N^{13}C labeled GB1 protein. The experimental time was 2h15 m for the ^{15}N-detected hCaN. The ^{1}H detected experiments were acquired during 25 h and approximately 4 days for the linearly sampled and the 26% non-uniformly sampled experiments, respectively. The conventional 3D HCaN NMR experiments (Wang et al. 1995) were recorded on a Varian Inova spectrometer using the default pulse sequence provided in BioPack. (**b**) and (**c**) 2D ^{15}N detected hCaN experiment of HEAT2 domain of human eIF4G and NFAT1 (SP3), respectively

Acquiring a uniformly sampled 3D experiment with the same resolution in the indirect dimensions as we obtain in the 2D would take weeks. By sacrificing considerable resolution, we were able to obtain a linearly sampled 3D HCaN NMR spectrum within 25 h. Figure 3a (center) shows a ^{13}Ca–^{15}N 2D projection of the conventional "out-and-back" 3D HCaN NMR experiment. Alternatively, non-uniform sampling permits us to approach the resolution of the 2D experiment in a reasonable amount of time. The ^{13}Ca–^{15}N 2D projection of the high-resolution, non-uniformly sampled 3D HCaN NMR spectrum is shown in the right panel of Fig. 3a. In this case we were able to obtain the same spectral parameters, including indirect ^{15}N resolution, in $\sim$4 days, with only 26% of the necessary grid points otherwise required for a linear sampling scheme. It shows that although an impressive time reduction can be achieved by using nonlinear sampling, the 2D ^{15}N detected Ca–N spectra can be collected an order of magnitude faster. As NMR sensitivity continues to improve, and resolution becomes the bottleneck in acquisition times, this kind of experimental scheme becomes increasingly important.

In the 2D hCaN experiment, 1,032 (^{15}N, direct dimension) and 100 (^{13}C, indirect dimension) complex data points were recorded. Spectral widths were set to 2,540 and 3,770 Hz for ^{15}N and ^{13}C, respectively. For each increment, 16 scans were accumulated. The recycle delay was set to 1 s, leading to a total experiment time of 2 h 15 min. Cosine-apodization was applied to each FID, which was then zero-filled to 2,048 data points before Fourier transformation. The indirect dimensions were processed using cosine-apodization and zero-filling to 256 data points.

The conventional 3D HCaN experiment (Fig. 3a, center panel) was recorded with 1,024 complex data points in the direct (^{1}H) dimension, and with 60 and 90 complex data points in the ^{15}N and ^{13}C indirect dimensions, respectively. For each increment, 4 scans were accumulated, with a recycle delay of 0.8 s, leading to a total experiment time of 25 h. In the direct dimension, a cosine-apodization function was applied for each FID, followed by zero-filling to 2,048 data points and Fourier transformation. Both indirect dimensions were processed using a cosine-apodization function and zero-filling to 128 data points. Spectral widths

were set to 1,800 and 3,750 Hz for ^{15}N and ^{13}C, respectively.

The 3D HCaN experiment using non-uniform sampling (Fig. 3b, right panel) was recorded with 1,024 complex data points in the direct (^{1}H) dimension, and with a sampling grid of 720 and 90 complex data points in the ^{15}N and ^{13}C indirect dimensions, respectively. A randomized non-uniform sampling schedule was generated using Poisson-gap sampling (Hyberts et al. 2010) and 17,318 points out of a possible 64,800 were collected, for a sampling density of 26.7%. For each increment, 4 scans were accumulated, with a recycle delay of 1.0 s, leading to a total experiment time of 4 days, 2 h and 15 min. Spectral widths were set to 1,800 and 3,750 Hz for ^{15}N and ^{13}C, respectively. In the direct dimension, a cosine-apodization function was applied to each FID, followed by zero-filling to 2,048 data points and Fourier transformation. The region from 2.5 to 6.2 ppm was extracted for subsequent reconstruction of the indirect dimensions by iterative soft thresholding (IST) (Hyberts et al. to be published). Both indirect dimensions were then processed using cosine apodization, zero filling, and Fourier transformation.

Notably, a narrower window was collected for ^{15}N in the 3D ^{1}H detected experiments than in the hCaN experiment in order to maximize resolution of the indirect dimension. Although similar results could be obtained with ^{13}C direct detection, as shown by Takeuchi et al. (2010), in this case, no post-processing manipulations are required to eliminate the ^{13}C–^{13}C coupling that occurs during direct carbon observation.

NMR assignment based on hCaN spectra

Figure 3b shows a 2D hCaN spectrum acquired on the 22 kDa HEAT2 domain of human translation initiation factor 4G (eIF4G). This domain mediates binding to the RNA helicase eIF4A and is involved in regulating protein synthesis (Marintchev et al. 2009). This experiment was recorded with the same spectral parameters as for GB1, except the number of scans per increment, which was set to 120, resulting in a total time of 15 h 30 min. Although deuteration is typically necessary for large proteins due to the ^{13}Ca–^{15}N magnetization transfer step, it shows that this experiment is still applicable for mid-size protonated proteins. Since the resonance assignments for this domain were previously known from conventional HN-detected 3D NMR experiments, we have used this as a model to test the ability of this kind of experiment to provide sequential backbone assignment information. A stretch of 5 sequential amino acids is indicated, including a proline, which cannot be seen in a conventional HN detected NMR experiment, and had not previously been assigned. Even though low-γ detection can not substitute ^{1}H detection, this type of experiment can be a useful part of an arsenal of backbone assignment experiments, when supplemented by other low-γ and ^{1}H detection experiments,.

Figure 3c shows an hCaN spectrum recorded on part of the regulatory domain of Nuclear Factor of Activated T-Cells (NFAT1). This transcription factor is rich in Serine-Proline (SP) sequence repetitions, and includes numerous phosphorylation sites. These segments are hard to detect and assign in conventional HN-based NMR experiments, due both to the limited proton and carbon dispersion and to the lack of an amide proton on prolines. The hCaN spectrum shown here provides spectral information about the SP3 region of this transcription factor and enables us to assign the connectivities of the prolines along the protein backbone, including some amino acids which can not be observed by HN-detected experiment. To illustrate such a correlation, the connectivity of peaks corresponding to a P-Q-P segment in the polypeptide amino acid sequence is shown. This segment cannot be assigned by HN-type experiments. In order to achieve high enough sensitivity for both inter- and intraresidue cross peaks, this last experiment was measured for 72 h on a ca. 300 uM sample.

Sensitivity improvement of hCaN versus the CaN experiment

Starting an experiment using proton polarization not only increases sensitivity due to the higher proton polarization, but also allows one to accumulate more scans per unit time because the natural longitudinal relaxation is shorter for protons than for carbon nuclei in proteins. Since the sensitivity is proportional to the square root of the number of scans, in theory the SNR of such spectra in comparison to the CaN experiments should be proportional to $\frac{\gamma H}{\gamma C} \cdot \sqrt{\frac{T1c}{T1H}} \cdot e^{-\Delta/T2(H\alpha)}$ (Ernst et al. 1987). In this equation, Δ represents the ^{1}H–^{13}C transfer time that is used during the initial INEPT. Figure 4 shows a comparison of the signal to noise ratio of two experiments which were acquired using the same experimental parameters and the same experiment time. The recycle delay was set to 1 s in the hCaN experiment and to 3 s in the CaN experiment, resulting in three-fold more scans being collected in the hCaN experiment. The experiments were acquired with a full Ca–N refocusing time, which leads to glycine signal cancellation in the hCaN experiment. On average, the hCaN experiment is roughly five times more sensitive than the CaN experiment. Furthermore, due to the relatively short period of the initial H–C transfer, even higher molecular-weight proteins will exhibit a significant improvement in SNR relative to the CaN experiment, as long as the transverse relaxation is roughly $T2(H\alpha) \geq \frac{1}{2JCH}$. However, due to the long Ca–N

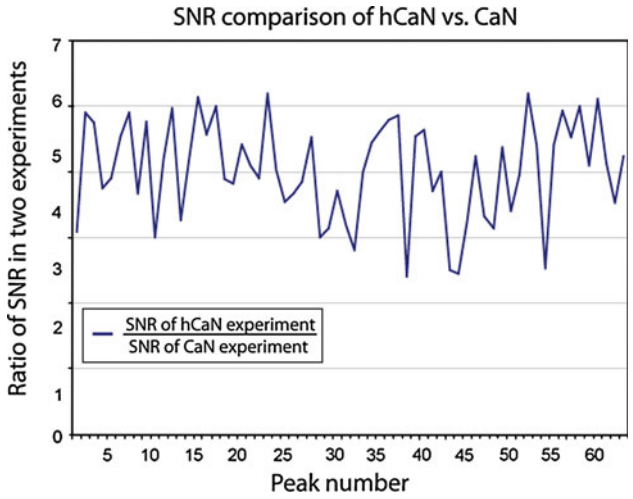

Fig. 4 Signal-to-noise ratio comparison of the 2D NMR hCaN versus the CaN experiment for selected peaks in the GB1 protein spectrum. The hCaN experiment is five times more sensitive on average than its counterpart that starts on the alpha carbon

transfer, very large proteins may relax too fast to complete this last step if the Ca's are protonated.

Discussion

We have presented here a new type of experiment for correlating protein ^{15}N resonances to neighboring alpha carbons, using ^{15}N direct detection NMR spectroscopy. We have improved the sensitivity so that this kind of experiment can now be acquired faster, on the order of few hours. Continued improvements in hardware and other techniques that improve SNR can make this kind of method a viable alternative, especially in cases that are poorly suited to conventional proton detection. Although nitrogen has the lowest gyromagnetic ratio of all backbone atoms, there are many advantages associated with it. In particular, resolutions of better than 1 Hz can be achieved due to the slow ^{15}N FID decay. Furthermore, an experiment that utilizes Ha rather than amide protons can in general be executed under a much broader range of pH values. This is of particular importance when studying unfolded proteins at physiological pH, since rapid exchange of exposed amide protons with water results in severe line-broadening. Additionally, the dimensions shown in the hCaN spectrum have better signal dispersion than amide protons for typical unfolded proteins.

Previously, we have shown that the sensitivity of nitrogen detection is comparable to carbon detection experiments and can be even better due to the lack of splitting complexities (Takeuchi et al. 2010). Although carbon resolution in the indirect dimension is limited by the C_α–C_β constant time period, which is implemented in the ^{15}N direct detection experiment, the use of alternating labeling schemes with 2-^{13}C glycerol or pyruvate can improve this resolution as well. A further improvement in sensitivity can be achieved by recording an IPAP type of experiment. This can allow for dissolving the protein in H_2O without the need for actual ^{1}H decoupling during acquisition, leading for further sensitivity improvement, by using an optimized longitudinal relaxation NMR technique (Pervushin et al. 2002; Schanda et al. 2005). Another similar option is the use of paramagnetic relaxation agents, which allows faster recycling without affecting the signal line width (Cai et al. 2006). Optimization of such experiments are currently an on-going topic of research in our lab.

These improvements, combined with the superior line width and dispersion that a ^{15}N-detection experiment offers, can make the hCaN experiment a powerful spectroscopy tool. The hCaN experiment can be applied not only to proteins but also for 2D NMR spectra of nucleic acids, where it may be particularly helpful due to proton exchange in hydrogen bonds between nucleotides in base pairs. We also look forward to pursuing the extension of the hCaN experiment to a higher dimensional NMR spectroscopy module and to applying this kind of experiment to the study of phosphorylation processes.

Acknowledgments This research was supported by the NIH grants GM047467, AI037581 and CA127990. Maayan Gal would like to thank the Human Frontier science Program (HFSP) for a postdoctoral fellowship. The authors would like to thank Dr. Gregory Heffron for fruitful discussions and technical assistance with the ^{15}N direct detection setup.

References

Bermel W, Bertini I, Felli IC, Kummerle R, Pierattelli R (2006a) Novel C-13 direct detection experiments, including extension to the third dimension, to perform the complete assignment of proteins. J Magn Reson 178:56–64

Bermel W, Bertini I, Felli IC, Lee Y-M, Luchinat C, Pierattelli R (2006b) Protonless NMR experiments for sequence-specific assignment of backbone nuclei in unfolded proteins. J Am Chem Soc 128:3918–3919

Bermel W, Bertini I, Felli IC, Piccioli M, Pierattelli R (2006c) C-13-detected protonless NMR spectroscopy of proteins in solution. Prog Nucl Magn Reson Spectrosc 48:25–45

Bertini I, Luchinat C, Parigi G and Pierattelli R (2008) Perspectives in paramagnetic NMR of metalloproteins. Dalton Trans 29: 3782–3790

Cai S, Seu C, Kovacs Z, Sherry AD, Chen Y (2006) Sensitivity enhancement of multidimensional NMR experiments by paramagnetic relaxation effects. J Am Chem Soc 128:13474–13478

Cavanagh J, Fairbrother WJ, Palmer AG, Skelton NJ (1996) Protein NMR Spectroscopy: principles and practice. Academic Press, San Diego

Emsley L, Bodenhausen G (1992) Optimization of shaped selective pulses for NMR using a quaternion description of their overall propagators. J Magn Reson 97:135–148

Ernst RR, Bodenhausen G, Wokaun A (1987) Principles of nuclear magnetic resonance in one and two dimensions. Oxford Univ Press, London/New York

Felli IC, Brutscher B (2009) Recent advances in solution NMR: fast methods and heteronuclear direct detection. Chem Phys Chem 10:1356–1368

Frueh DP, Arthanari H, Wagner G (2005) Unambiguous assignment of NMR protein backbone signals with a time-shared triple-resonance experiment. J Biomol NMR 33:187–196

Hoult DI (1978) The NMR receiver: a description and analysis of design. Prog Nucl Magn Reson Spectrosc 12:41–77

Howarth OW, Lilley DMJ (1978) Carbon-13-NMR of peptides and proteins. Prog Nucl Magn Reson Spectrosc 12:1–40

Hyberts SG, Takeuchi K, Wagner G (2010) Poisson-gap sampling and forward maximum entropy reconstruction for enhancing the resolution and sensitivity of protein NMR data. J Am Chem Soc 132:2145–2147

Hyberts SG, Wagner AB, Milbradt A, Arthanari H, Wagner G Fast reconstruction by iterative soft thresholding of multidimensional non-uniformly sampled NMR data sampled with multidimensional poisson gap scheduling (to be published)

John M, Park AY, Dixon NE, Otting G (2007) NMR detection of protein N-15 spins near paramagnetic lanthanide ions. J Am Chem Soc 129:462–463

Kupce E, Freeman R (1995) Adiabatic pulses for wideband inversion and broadband decoupling. J Magn Reson A 115:273–276

Lee D, Vogeli B, Pervushin K (2005) Detection of C‘ C-alpha correlations in proteins using a new time- and sensitivity-optimal experiment. J Biomol NMR 31:273–278

Levitt MH (2001) Spin dynamics. Wiley, New York

Levy GC, Lichter RL (1979) Nitrogen-15 nuclear magnetic resonance spectroscopy. Wiley, New York

Lin IJ, Xia B, King DS, Machonkin TE, Westler WM, Markley JL (2009) Hyperfine-shifted C-13 and N-15 NMR signals from Clostridium pasteurianum rubredoxin: extensive assignments and quantum chemical verification. J Am Chem Soc 131:15555–15563

Mantylahti S, Aitio O, Hellman M, Permi P (2010) HA-detected experiments for the backbone assignment of intrinsically disordered proteins. J Biomol NMR 47:171–181

Marintchev A, Edmonds KA, Marintcheva B, Hendrickson E, Oberer M, Suzuki C, Herdy B, Sonenberg N, Wagner G (2009) Topology and regulation of the human eIF4A/4G/4H helicase complex in translation initiation. Cell 136:447–460

Marion D, Ikura M, Tschudin R, Bax A (1989) Rapid recording of 2d Nmr-spectra without phase cycling—application to the study of hydrogen-exchange in proteins. J Magn Reson 85:393–399

Mishkovsky M, Frydman L (2004) Sensitivity enhancement in 1D heteronuclear NMR spectroscopy via single-scan inverse experiments. Chem Phys Chem 5:779–786

Morris GA, Freeman R (1979) Enhancement of nuclear magnetic resonance signals by polarization transfer. J Am Chem Soc 101:760–762

Pervushin K (2000) Impact of transverse relaxation optimized spectroscopy (TROSY) on NMR as a technique in structural biology. Q Rev Biophys 33:161–197

Pervushin K, Riek R, Wider G, Wuthrich K (1997) Attenuated T-2 relaxation by mutual cancellation of dipole–dipole coupling and chemical shift anisotropy indicates an avenue to NMR structures of very large biological macromolecules in solution. Proc Natl Acad Sci USA 94:12366–12371

Pervushin K, Vogeli B, Eletsky A (2002) Longitudinal (1)H relaxation optimization in TROSY NMR spectroscopy. J Am Chem Soc 124:12898–12902

Schanda P, Kupce E, Brutscher B (2005) SOFAST-HMQC experiments for recording two-dimensional heteronuclear correlation spectra of proteins within a few seconds. J Biomol NMR 33:199–211

Shaka AJ, Keeler J (1987) Broadband spin decoupling in isotropic liquids. Prog Nucl Magn Reson Spectrosc 19:47–129

Takeuchi K, Sun ZY, Wagner G (2008) Alternate 13C–12C labeling for complete mainchain resonance assignments using C alpha direct-detection with applicability toward fast relaxing protein systems. J Am Chem Soc 130:17210–17211

Takeuchi K, Heffron G, Sun ZYJ, Frueh DP, Wagner G (2010) Nitrogen-detected CAN and CON experiments as alternative experiments for main chain NMR resonance assignments. J Biomol NMR 47:271–282

Tamiola K, Mulder FAA (2011) ncIDP-assign: a SPARKY extension for the effective NMR assignment of intrinsically disordered proteins. Bioinformatics 27:1039–1040

Tompa P (2003) Intrinsically unstructured proteins evolve by repeat expansion. Bioessays 25:847–855

Tugarinov V, Hwang PM, Ollerenshaw JE, Kay LE (2003) Cross-correlated relaxation enhanced 1H–13C NMR spectroscopy of methyl groups in very high molecular weight proteins and protein complexes. J Am Chem Soc 125:10420–10428

Vance CK, Kang YM, Miller AF (1997) Selective N-15 labeling and direct observation by NMR of the active-site glutamine of Fe-containing superoxide dismutase. J Biomol NMR 9:201–206

Vasos PR, Hall JB, Kummerle R, Fushman D (2006) Measurement of N-15 relaxation in deuterated amide groups in proteins using direct nitrogen detection. J Biomol NMR 36:27–36

Venters RA, Huang CC, Farmer BT, Trolard R, Spicer LD, Fierke CA (1995) High-Level H-2/C-13/N-15 labeling of proteins for Nmr-Studies. J Biomol NMR 5:339–344

Wang AC, Grzesiek S, Tschudin R, Lodi PJ, Bax A (1995) Sequential backbone assignment of isotopically enriched proteins in D_2O by deuterium-decoupled HA(CA)N and HA(CACO)N. J Biomol NMR 5:376–382

Wuthrich K, Wagner G (1979) Nuclear magnetic resonance of labile protons in the basic pancreatic trypsin inhibitor. J Mol Biol 130:1–18

Xu J, Millet O, Kay LE, Skrynnikov NR (2005) New spin probe of protein dynamics: Nitrogen relaxation in N-15-H-2 amide groups. J Am Chem Soc 127:3220–3229

Zhou P, Lugovskoy AA, Wagner G (2001) A solubility-enhancement tag (SET) for NMR Studies of poorly behaving proteins. J Biomol NMR 20:11–14